Archive of Applied Mechanics (2023) 93:1491–1505
https://doi.org/10.1007/s00419-022-02341-9

ORIGINAL

Wenjie Guo · Xian Hong · Yueyang Han · Tianyun Li · Xiang Zhu

Vibration and far-field sound radiation of a horizontal, finite-long cylindrical shell partially submerged in fluid

Received: 15 July 2022 / Accepted: 5 December 2022 / Published online: 4 February 2023

Abstract The vibroacoustic study of a horizontal, finite-long cylindrical shell partially submerged in a fluid is presented in this paper. First, the mathematical and physical model of the system is established using two different coordinate systems for the sound field and the structure. Second, using the Galerkin method to deal with the continuity condition for the velocity on the acoustic–structure coupling surface, the matrix relation of the coefficient vector of the sound field and the displacement field is obtained, followed by the analytical solution of the vibration. The accuracy of this new method is verified through numerical simulations, while its broad applicability and reduced computational cost are demonstrated. Moreover, the method is extended to obtain the far-field sound radiation using the stationary phase method. Altogether, the present work introduces a new thought for solving the vibroacoustic characteristics of a partially coupled system consisting of elastic structures and external fluid fields.

Keywords Partially submerged · Finite-long cylindrical shell · Vibration · Far-field sound radiation · Free surface

1 Introduction

Cylindrical shells are widely used in naval architecture and ocean engineering due to their excellent geometric and mechanical properties, e.g., the main hull structures of submarines, ocean pipelines, some liquid storage containers, etc., are cylindrical shells. With the development of science and technology, the requirements for vibroacoustic quality are becoming increasingly strict, and the basic requirements for strength, stiffness, and stability. Therefore, research on the vibroacoustic properties of underwater cylindrical shells has been an essential field of naval architecture and ocean engineering. Besides, the vibroacoustic properties of underwater cylindrical shells have attracted the attention of many researchers.

Xian Hong, Tianyun Li and Xiang Zhu have contributed equally to this work.

W. Guo · X. Hong
Engineering Research Center of Railway Environment Vibration and Noise Ministry Education, East China Jiaotong University, Nanchang 330013, China

W. Guo · Y. Han (✉) · T. Li · X. Zhu
School of Naval Architecture and Ocean Engineering, Huazhong University of Science & Technology, Wuhan 430074, China
e-mail: husthyy2012@foxmail.com

Y. Han · T. Li · X. Zhu
Hubei Key Laboratory of Naval Architecture and Ocean Engineering Hydrodynamics, Wuhan 430074, China

T. Li · X. Zhu
Collaborative Innovation Center for Advanced Ship and Deep-Sea Exploration, Shanghai 200240, China

For decades, a large number of studies on the vibroacoustic characteristics of submerged or fluid-filled cylindrical shells have been reported, the previous studies focused mainly on cylindrical shells which were fully filled with liquid [1, 2] or completely submerged in the fluid domain (infinite domain [3, 4], half-space domain [5, 6], quarter-space domain [7, 8], etc.). So that the cylindrical shells were in complete contact with the surrounding fluid, and the circumferential discontinuity of the fluid load on the shell surface was not taken into account. However, cylindrical shells partially coupled with external/internal fluid (the shell centerline is parallel to the free surface) are frequently encountered in engineering, e.g., tanks containing oil, pipes conveying fluid, and ship or submarines floating on the sea. The studies on the vibroacoustic characteristics of shells partially coupled with fluid still receive scant attention compared with those of shells fully coupled with the surrounding fluid.

In some cases, a better understanding of the vibroacoustic behaviors for a partial shell-liquid coupling system is urgent to keep perfect dynamic performance. In previous studies, numerical methods [9–14] are the most commonly used methods, such as the finite element method (FEM), boundary element method (BEM), and boundary integral method (BIM). However, no matter from an aspect of verifying numerical methods or revealing the characteristics of a fluid–structure interaction system in the mechanism, developing an analytical or semi-analytical approach is necessary [15–19].

In the theoretical research of the vibroacoustic characteristics of partial cylindrical shell-liquid coupling systems, the models of semi-liquid-filled or semi-submerged cylindrical shells are just exceptional cases [20, 21]. That is because when the free surface of the fluid and the shell centerline are coplanar, the analytical expression of the fluid load is easy to achieve by adopting sine series to meet the free surface boundary condition automatically.

For more general cases, such as free surface and shell centerline are non-coplanar, there are currently two commonly used approximate analytical methods. One method is presented by Ergin [22] and Selmane [23], which ignores the influence of the free surface, so it is convenient to obtain an analytical expression of the fluid velocity potential, and it applies to any submerged depth. However, the calculation results are not accurate enough, and the relative error of the natural frequencies can reach more than ten percent. The other one is presented by Amabili [24, 25], which replaces the free surface boundary with two hypotenuse boundaries. However, to ensure the accuracy of results, the wet angle of the partially coupled system is limited to between 3/4 and 5/4 in his work. Besides, other scholars [26–28] studied the free vibration characteristics or the added mass effects of partially fluid-filled circular tubes by the experimental method. However, the experimental method is difficult to analyze the dynamic mechanism of partial shell-liquid coupling systems.

It can be seen from the above references that it is difficult to take into account the range of applications and accuracy of the method simultaneously for the analytical or semi-analytical study of partial coupling problems. This is because the sound field's coordinate origin often coincides with the coordinate origin of the structural displacement field, regardless of whether the cylindrical shell is semi-fluid-filled, fully fluid-filled, semi-submerged, or submerged in an infinite domain. Therefore, in the partial coupling problem analysis, the researchers will habitually set the coordinate origin of the sound field and the structural displacement field at the same point (center of the circle). As a result, the free surface boundary condition will be challenging to handle and can only be ignored or approximately replaced.

The first is to break through the shackles of inertial thought to overcome the above deficiencies. The authors proposed a new method [29, 30] to solve the vibroacoustic characteristics of two-dimensional cylindrical shells partially coupled with internal or external fluids. Its core idea is to use the Galerkin method to establish the sound field and structural displacement field in two coordinate systems and obtain the mathematical relationship between the structural and sound fields. Expressly, the coordinate origin of the sound field is set on the free surface, and the sinusoidal trigonometric series is adopted to satisfy the sound pressure release boundary condition. Meanwhile, the motion equation of the shell is established in a coordinate system with a cylindrical center as the coordinate origin. Then, the Galerkin method is applied to deal with the continuous condition at the acoustic–structure interaction interface. Therefore, the relationship between the acoustic and structure fields can be obtained. Based on our method, Zhao et al. [20] further studied the sound radiation of an infinite-long cylindrical shell submerged partially in fluid and subject to a point harmonic excitation.

In order to further expand our previous work to a 3-D model, we study a finite-long cylindrical shell with both ends simply supported. And the influence of structural axial bending waves is considered by applying the trigonometric series expansion. Then, the free and forced vibration analysis model is established by combining two sets of coordinate systems and the Galerkin method. Finally, the vibration analysis model is solved, and the relationship between vibration characteristics and immersion depth is also analyzed. In addition, the present

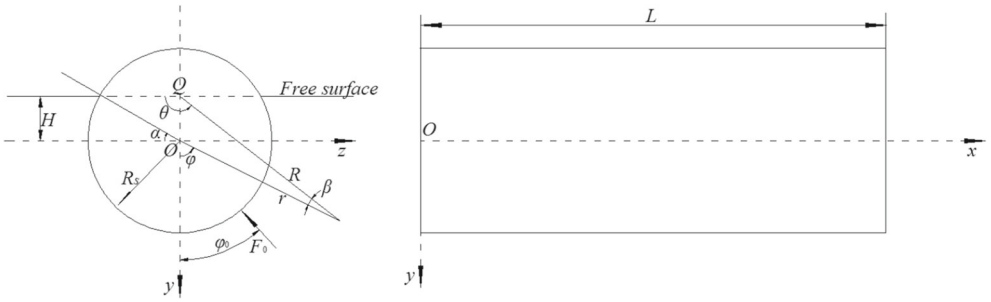

Fig. 1 The cylindrical coordinate systems of the physical model

method is extended to obtain the far-field sound radiation by combining the stationary phase method and the Fourier transform technique.

2 Theoretical analysis of fluid–structure coupling vibration

2.1 The physical model

As shown in Fig. 1, a finite-long cylindrical shell of these parameters, length L, thickness h, radius R_s, Young's modulus E, Poisson's ratio μ, and density ρ, is considered to be partially submerged in a fluid with the density ρ_f and the sound velocity c_f. The fluid domain is assumed to be semi-infinite and bounded by a free surface, and the space above the free surface is considered a vacuum.

The cylindrical coordinate systems (x, r, φ) and (x, R, θ) are assumed to be the structural and the acoustical coordinate systems of this model ($0 \le \varphi \le 2\pi$ and $0 \le \theta \le \pi$), respectively, which are used to deduce theoretical equations. The origins of these two coordinate systems are O (the center of the circular cylindrical shell) and Q (the intersection of the y-axis and the free surface), respectively. The opposite of the y-coordinate value of point Q is defined as$H$ ($-R_s \le H \le R_s$), which denotes the free surface's height. So the immersion depth equals $R_s + H$, and the non-dimensional immersion depth $L_d = (R_s + H)/(2R_s)$. f_0 is a harmonic point force exciting on the cylindrical shell with amplitude F_0 and frequency f at (Rs, x_0, φ_0) in the axial direction. α ($\sin\alpha = H/R_s$) represents the angle between the x-axis and $\vec{r}$ direction, and β is the angle between $\vec{R}$ and $\vec{r}$.

2.2 The fluid field model and fluid field boundary conditions

In Sect. 2.1, the physical model is considered a typical sound–structure coupling model. The key points are how to express the sound pressure p, which can satisfy the corresponding boundary conditions. Therefore, an independent acoustical coordinate system is introduced to address this problem.

Assuming that the liquid around the shell is an acoustic medium, the sound pressure p should satisfy the acoustic Helmholtz equation:

$$\nabla^2 p + k_f^2 p = 0 \tag{1}$$

where $k_f = \omega / c_f$ is the acoustic wave number, $\omega = 2\pi f$ is the circular frequency, and ∇^2 denotes the Laplace operator.
In addition, the sound pressure p needs to satisfy the Sommerfeld condition at infinity field:

$$\lim_{R\to\infty} [R(\partial p / \partial R - ik_f p)] = 0 \tag{2}$$

where $i = \sqrt{-1}$ denotes the imaginary unit.
On the free surface, the sound pressure release boundary condition can be expressed as follows:

$$p = 0, \text{ on the free surface} \tag{3}$$

Since the origin of the acoustical coordinate system is established on the free surface, all the above boundary conditions can be satisfied by constructing sine series and Bessel functions as follows:

$$p(R,\theta,x)=\sum_{m=1}^{+\infty}\sum_{j=1}^{+\infty}A_{m,j}K_j(k_rR)\sin(j\theta)\sin(k_mx) \tag{4}$$

where m and j are the expansion coefficients and $A_{m,j}$ is the function of sound pressure amplitude. $K_j()$ is the jth-order fixed Bessel function of the second kind, $k_r=\sqrt{k_m^2-k_f^2}$ is the radial wavenumber and $k_f=\omega/c_f$ is the compression wavenumber, $\omega=2\pi f$ is the circular frequency, and f is the frequency of the time-harmonic surface velocity distribution. However, $k_f>k_m$ $k_r=\sqrt{k_f^2-k_m^2}$, and $K_j()$ should be placed by the jth-order Hankel function of the first kind $H_j^{(1)}()$.

2.3 The governing equations of the cylindrical shell

After deriving the analytical expression of the sound pressure, the governing equations of the sound–structure coupling system could be obtained. The Flügge shell equations [5] are applied to depict the motions of the cylindrical shell:

$$[\mathbf{L}]\begin{bmatrix}u\\v\\w\end{bmatrix}=\frac{(1-\mu^2)R_s^2}{Eh}\begin{bmatrix}0\\0\\f_r-f_p\end{bmatrix} \tag{5}$$

where u, v, and w are the displacements of the shell in the axial, tangential, and radial directions, respectively. f_p is the acoustic load which is imposed by the liquid on the inner surface of the shell, $[\mathbf{L}]$ represents the classical Flügge differential operator for the thin shell theory:

$$L_{11}=R_s^2\tfrac{\partial^2}{\partial x^2}+\tfrac{1-\mu}{2}(K+1)\tfrac{\partial^2}{\partial\varphi^2}-\tfrac{\rho R_s^2(1-\mu^2)}{E}\tfrac{\partial^2}{\partial t^2},L_{12}=L_{21}=R_s\tfrac{1+\mu}{2}\tfrac{\partial^2}{\partial x\partial\varphi}$$

$$L_{13}=L_{31}=R_s\mu\frac{\partial}{\partial x}-KR_s^3\frac{\partial^3}{\partial x^3}+KR_s\frac{1-\mu}{2}\frac{\partial^3}{\partial x\partial\varphi^2}$$

$$L_{22}=R_s^2\frac{1-\mu}{2}(3K+1)\frac{\partial^2}{\partial x^2}+\frac{\partial^2}{\partial\varphi^2}-\frac{\rho R_s^2(1-\mu^2)}{E}\frac{\partial^2}{\partial t^2}$$

$$L_{23}=L_{32}=\frac{\partial}{\partial\varphi}-KR_s^2\frac{3-\mu}{2}\frac{\partial^3}{\partial x^2\partial\varphi}$$

$$L_{33}=1+K+2K\frac{\partial^2}{\partial\varphi^2}+K\nabla^4+\frac{\rho R_s^2(1-\mu^2)}{E}\frac{\partial^2}{\partial t^2}$$

$$\nabla^4=(R_s^4\tfrac{\partial^4}{\partial x^4}+2R_s^2\tfrac{\partial^4}{\partial x^2\partial\varphi^2}+\tfrac{\partial^4}{\partial\varphi^4}),K=h^2/12R_s^2.$$

As the shell structure and the fluid are coupled partially, the acoustic load f_p imposed on the shell could be expressed in the forms of piecewise functions:

$$f_p=\begin{cases}p|_{r=R_s}, & -\frac{\pi}{2}-\alpha\le\varphi\le\frac{\pi}{2}+\alpha\\ 0, & \text{the others}\end{cases} \tag{6}$$

Assuming that the cylindrical shell is excited by a point harmonic force at (x_0, Rs, φ_0), and the force f_r could be described as [31]:

$$f_r(x,\varphi)=\frac{F_0}{R_s}\delta(x-x_a)\delta(\varphi-\varphi_0) \tag{7}$$

where $\delta()$ represents the Delta function.

Therefore, u, v, w, f_p, and f_r could be written in the following forms, respectively:

$$\begin{cases} u = \sum_{m=1}^{+\infty} \sum_{n=-\infty}^{+\infty} U_{mn} \cos(k_m x) \exp(in\varphi) \\ v = \sum_{m=1}^{+\infty} \sum_{n=-\infty}^{+\infty} V_{mn} \sin(k_m x) \exp(in\varphi) \\ w = \sum_{m=1}^{+\infty} \sum_{n=-\infty}^{+\infty} W_{mn} \sin(k_m x) \exp(in\varphi) \\ f_r = \sum_{m=1}^{+\infty} \sum_{n=-\infty}^{+\infty} F_{mn} \sin(k_m x) \exp(in\varphi) \\ f_p = \sum_{m=1}^{+\infty} \sum_{n=-\infty}^{+\infty} f_{mn} \sin(k_m x) \exp(in\varphi) \end{cases} \tag{8}$$

where U_{mn}, V_{mn}, and W_{mn} are amplitudes of the displacements in the axial, tangential, and radial directions, respectively. F_{mn} and f_{mn} are the amplitudes of f_r and f_p, respectively. m and n are the expansion coefficient.

Substituting Eq. (4) and Eq. (7) into Eq. (8), respectively, and then conducting the orthogonal processing, the expression of f_{mn} and F_{mn} is obtained:

$$f_{mn} = \sum_{j=1}^{+\infty} \frac{1}{2\pi} \int_{-\frac{\pi}{2}-\alpha}^{\frac{\pi}{2}+\alpha} A_{m,j} K_j(k_r R) \sin(j\theta) \exp(-in\varphi) \mathrm{d}\varphi \tag{9}$$

$$F_{mn} = \frac{F_0 sin(k_m x_0) \exp(-in\varphi_0)}{L R_s \pi} \tag{10}$$

As shown in Fig. 1, the geometrical relations between the structural and the acoustical coordinate systems can be learned:

$$\begin{cases} R\sin\theta + r\cos\varphi = H \\ R\cos\theta + r\sin\varphi = 0 \end{cases} \tag{11}$$

Therefore, for an arbitrary point on the fluid–structure interface ($r = R_s$), Eq. (11) can be turned into the following forms:

$$\begin{cases} R = \sqrt{H^2 - 2HR_s\cos\varphi + R^2} \\ \theta = arcos\left(-\dfrac{R_s\sin\varphi}{R}\right) \end{cases} \tag{12}$$

Because the Bessel function exists in Eq. (9), the integral of f_{mn} cannot be calculated directly by substituting Eq. (12) into Eq. (9). The discrete method is employed to address this problem. The integral domain is divided into K segments, and the value of the function at the midpoint of each segment is substituted into the summation formula:

$$\int_{-\alpha-\frac{\pi}{2}}^{\alpha+\frac{\pi}{2}} F(\varphi)\mathrm{d}\varphi = \sum_{k=1}^{K} F(\varphi_k)\Delta\varphi, \quad \Delta\varphi = \frac{\pi + 2\alpha}{K}, \quad \varphi_k = -\frac{\pi}{2} - \alpha + (k - 0.5)\Delta\varphi \tag{13}$$

where $F(\varphi)$ denotes the integral function in Eq. (9). When $K = 100$, the discrete method makes the integral convergent.

In the same way, by substituting Eq. (8) into (5) and conducting the orthogonal processing, the decoupling motion equations of the cylindrical shell are obtained:

$$[T]\begin{bmatrix} U_{mn} \\ V_{mn} \\ W_{mn} \end{bmatrix} = \frac{(1-\mu^2)R_s^2}{Eh}\begin{bmatrix} 0 \\ 0 \\ F_{mn} - f_{mn} \end{bmatrix} \tag{14}$$

where the elements of matrix $[\boldsymbol{T}]$ are: $\zeta = k_m R_s, T_{11} = \Omega^2 - \zeta^2 - n^2(1+K)(1-\mu)/2, T_{12} = i\zeta n(1+\mu)/2, T_{13} = \mu\zeta + K\zeta^3 - K(1-\mu)\zeta n^2/2, T_{21} = -T_{12}, T_{22} = \Omega^2 - \zeta^2(1+3K)(1-\mu)/2 - n^2, T_{23} = in + iKn\zeta^2(3-\mu)/2, T_{31} = -T_{13}, T_{32} = T_{23}, T_{33} = 1 + K + K\zeta^4 + 2Kn^2\zeta^2 + Kn^4 - 2Kn^2 - \Omega^2$. where $\Omega = \omega\sqrt{\rho R_s^2(1-\mu^2)/E}$ is the non-dimensional frequency.

From Eq. (14), one can obtain the sound–structure coupling equation related to the radial displacement [5]:

$$W_{mn} = \frac{I_{mn}\left(1-\mu^2\right)R_s^2}{Eh}(F_{mn} - f_{mn}) \tag{15}$$

where $I_{mn} = (T_{11}T_{22} - T_{12}T_{21})\big/ \det(\boldsymbol{T})$ and $\det(\boldsymbol{T})$ is the determinant of the matrix $[\boldsymbol{T}]$.

2.4 The treatment of the velocity continuity condition on the sound–structure interface

The relationship between the radial displacement amplitudes W_{mn} and the acoustic load amplitudes f_{mn} is the key to solving Eq. (15). Thus, it is essential to emphasize the coupling condition on the interface, and in particular, the radial velocity on the inner surface of the cylindrical shell should be equal to that of the fluid:

$$\frac{\partial^2 w}{\partial t^2} = -\frac{1}{\rho_f}\frac{\partial p}{\partial r}\bigg|_{r=R_s}, \text{ on the sound - structure interface} \tag{16}$$

The Galerkin method is employed here to deal with the velocity continuity Eq. (16). The optional weight functions are the circumferential function of the radial displacement of the cylindrical shell:

$$f_n(\varphi, x) = \exp(in\varphi)\sin(k_m x), \text{ Weight function} \tag{17}$$

By substituting Eqs. (17) into Eq. (16), the weak forms of the Galerkin integral are obtained:

$$\rho_f\omega^2\int_0^L\int_{-\alpha-\frac{\pi}{2}}^{\alpha+\frac{\pi}{2}} w(\varphi, x)\, f_n(\varphi, x)\mathrm{d}\varphi\mathrm{d}x = \int_0^L\int_{-\alpha-\frac{\pi}{2}}^{\alpha+\frac{\pi}{2}} \frac{\partial p(R,\theta,x)}{\partial r}\bigg|_{r=R_s} f_n(\varphi, x)\mathrm{d}\varphi\mathrm{d}x \tag{18}$$

where $n = [-N, -N+1, \ldots\ldots, N-1, N], j = [1, 2, \ldots\ldots, 2N, N+1]$, and N is the truncated number.
Since the axial integrals in Eq. (18) are decoupled, the relationship between the radial displacement amplitudes and the sound pressure amplitudes can be obtained at a given value of m:

$$\rho_f\omega^2[\boldsymbol{V_s}]\{\boldsymbol{W_{mn}}\} = [\boldsymbol{V_p}]\left\{\boldsymbol{A_{mj}}\right\} \tag{19}$$

where $[\boldsymbol{V_s}]$ and $[\boldsymbol{V_p}]$ are square matrices of $2N+1$ orders. $\{\boldsymbol{W_{mn}}\} = [W_{m,-N}, W_{m,-N+1}, \ldots\ldots, W_{m,N-1}, W_{m,N}]^T$ and $\{\boldsymbol{A_{mj}}\} = [A_{m,1}, A_{m,2}, \ldots\ldots, A_{m,2N}, A_{m,2N+1}]^T$ are amplitude vectors of the radial displacement and the sound pressure, respectively. The superscript T denotes matrix transposition.
Based on Eq. (11), the radial derivative of the sound pressure can be converted to that in the acoustical coordinate system:

$$\frac{\partial p}{\partial r} = \frac{\partial p}{\partial R}\cos\beta + \frac{\partial p}{\partial\theta}\frac{\sin\beta}{R} \tag{20}$$

where $\beta = 3\pi/2 - \theta - \varphi$.
Then, by using the weight function $\exp(in\varphi)$, the forms of elements in $[\boldsymbol{V_s}]$ and $[\boldsymbol{V_p}]$ are expressed as follows, respectively:

$$\begin{cases} [\boldsymbol{V_s}]_{a,b} = \int_{-\alpha-\frac{\pi}{2}}^{\alpha+\frac{\pi}{2}} \exp[i(b-1-N)\varphi]\cdot\exp[i(a-1-N)\varphi]\mathrm{d}\varphi \\ [\boldsymbol{V_p}]_{a,b} = \displaystyle\int_{-\alpha-\frac{\pi}{2}}^{\alpha+\frac{\pi}{2}} k_r K_b'(k_r R)\sin(b\theta)\cos\beta\cdot\exp[i(a-1-N)\varphi]\mathrm{d}\varphi \\ \qquad + \displaystyle\int_{-\alpha-\frac{\pi}{2}}^{\alpha+\frac{\pi}{2}} bK_b(k_r R)\cos(b\theta)\frac{\sin\beta}{R}\cdot\exp[i(a-1-N)\varphi]\mathrm{d}\varphi \end{cases} \tag{21}$$

where a and b denote the row and the column of matrices, respectively, and Eq. (21) should be worked out with the discrete method as Eq. (13), due to the difficulty of the Bessel functions.

Table 1 Comparison of the first-order natural frequencies at different L_d (unit: Hz)

Ld	0.1	0.2	0.3	0.4	0.5	0.6	0.7	0.8	0.9
PM	129.8	125.7	117. 0	112.9	111.4	109.6	107.2	105.9	105.0
FEM	129.5	125.6	117.0	113.0	111.5	109.7	107.3	106.0	105.2

2.5 The solution of the sound–structure coupling equation

For convenience, the sound–structure coupling Eq. (21) is converted to the matrix equation:

$$\frac{Eh}{(1-\mu)R^2}\{W_{mn}\} = [G](\{F_{mn}\} - \{f_{mn}\}) \tag{22}$$

where $\{\boldsymbol{F_{mn}}\} = F_0 sin(k_m x_0) \big/ (L R_s \pi) \cdot \{\exp(iN\varphi_0),\ \exp[i(N-1)\varphi_0],\ .....,\ \exp(-iN\varphi_0)\}^T$, $[\boldsymbol{G}]$ is the diagonal matrix, $[\boldsymbol{G}]_{j,j} = I_{m,\,j\text{-}1\text{-}N}$, $\{\boldsymbol{f_{mn}}\} = \{f_{m,-N},\ f_{m,-N+1},\ .....,\ f_{m,N}\}^T$.
Similarly, Eq. (9) is also converted to the matrix equation:

$$\{\boldsymbol{f_{mn}}\} = [\boldsymbol{T_p}]\{\boldsymbol{A_{mj}}\} \tag{23}$$

where the element in the matrix $[\boldsymbol{T_p}]$ is expressed as:

$$[\boldsymbol{T_p}]_{a,b} = \int_{-\alpha-\frac{\pi}{2}}^{\alpha+\frac{\pi}{2}} \exp[-i(a-1-N)\varphi] \cdot K_b^{(1)}(k_f R)\sin(b\theta)\mathrm{d}\varphi \tag{24}$$

By substituting Eqs. (19) and (23) into (22), the matrix equation related to the radial displacement $\{\boldsymbol{W_{mn}}\}$ is obtained:

$$\left(\frac{Eh}{R_s^2(1-\mu^2)}[\boldsymbol{J}] + \rho_f\omega^2[\boldsymbol{G}][\boldsymbol{T_p}][\boldsymbol{V_p}]^{-1}[\boldsymbol{V_s}]\right)\{\boldsymbol{W_{mn}}\} = [\boldsymbol{G}]\{\boldsymbol{F_{mn}}\} \tag{25}$$

where $[\boldsymbol{J}]$ is the unit matrix of $2N+1$ orders. With the exciting force $\{\boldsymbol{F_{mn}}\}$ being zero, a series of frequencies ω could be obtained by combining stepwise search and dichotomy.

The radial displacement can be obtained by solving the matrix Eq. (25). Then, by substituting $\{\boldsymbol{W_{mn}}\}$ into Eq. (19), $\{\boldsymbol{A_{mj}}\}$ can be obtained as well as the sound pressure. The value range of m is 1 to a truncated number M.

3 Numerical analysis

The following parameters of the coupling model are used in the calculation: $E = 206$GPa, $\mu = 0.3$, $\rho = 7850$ kg/m^3, $\rho_f = 1025$ kg/m^3, $c_f = 1500$ m/s, $L = 1.284$, $R_s = 0.18$ m, $h = 0.003$ m. The complex elastic modulus of the shell is expressed as $E' = E(1+i\eta)$, where the structural damping factor $\eta = 0.01$.

3.1 Application scope of the present method

In the previous work by Amabili [24], angle α is limited between $-\pi/8$ and $\pi/8$, and the corresponding limitation of the non-dimensional immersion depth L_d is from 0.31 to 0.69 approximately. However, the application range can be significantly expanded using this method. For verifying this advantage, the first-order natural frequencies calculated from the present method (PM) and the finite element method (FEM) are compared in Table 1 when $L_d = 0.1 \sim 0.9$ (this range covers most engineering practices). The cylindrical shell is divided into 2400 shell elements in the numerical simulation. The free and forced vibration of the partially submerged cylindrical shell can be solved by setting the fluid–structure interaction (FSI) surface and the immersion depth in MSC.Nastran with the virtual mass method.

It is shown in Table 1 that the natural frequencies of the first order obtained from the proposed method agree well with those from the FEM. Also, the scope of L_d is from 0.1 to 0.9, which shows a larger application scope of the present method than that proposed by Amabili [24].

Table 2 Comparison of the natural frequencies (Hz) between the present method and FEM at different L_d

Order	$L_d = 0.25$			$L_d = 0.5$			$L_d = 0.75$		
	f_{PM}	f_{FEM}	Error (%)	f_{PM}	f_{FEM}	Error (%)	f_{PM}	f_{FEM}	Error (%)
1	121.1	121.0	0.08	111.4	111.5	0.09	106.5	106.6	0.09
2	125.0	124.5	0.40	113.5	113.4	0.09	108.2	108.3	0.09
3	179.2	178.8	0.22	160.6	160.5	0.06	140.1	140.5	0.28
4	194.3	194.2	0.05	165.6	164.9	0.42	144.6	144.4	0.14
5	254.2	255.5	0.51	239.3	240.7	0.58	231.5	232.9	0.60
6	263.0	263.3	0.11	242.8	243.9	0.45	233.1	234.4	0.55
7	281.2	282.3	0.39	265.7	267	0.49	242.7	244.5	0.74
8	293.7	294.2	0.17	267.7	269.4	0.63	249.4	250.7	0.52
9	367.8	367.9	0.03	320.9	321.9	0.31	287.7	289.2	0.52
10	370.5	369.8	0.19	321.6	322.4	0.25	288.4	290	0.55

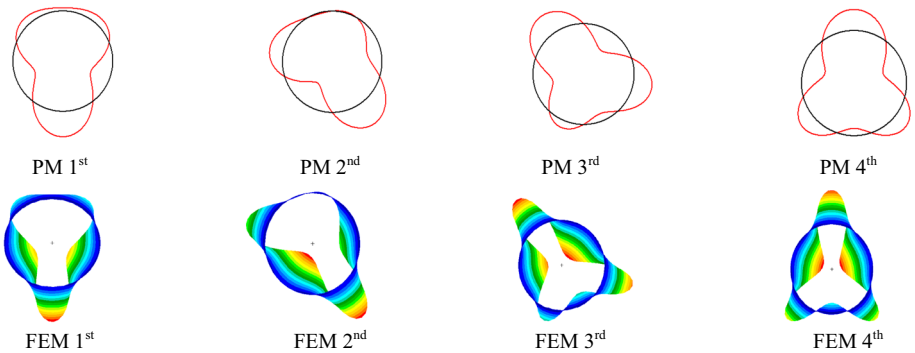

Fig. 2 The circumferential mode shapes of the first four orders when $L_{\mathrm{d}} = 0.75$

3.2 Accuracy verification of the present method

After analyzing the convergence and scope of application of the method, we further explore the accuracy of the present method. We take free vibration as an example. The first ten-order natural frequencies obtained with the present method and the numerical simulation are compared in Table 2 at different non-dimensional immersion depths ($L_d = 0.25$, 0.5 and 0.75), where f_{PM} and f_{FEM} represent the natural frequencies calculated with the present method and the FEM, respectively. The relative error of the natural frequencies between both methods is defined as Error $= | f_{\mathrm{PM}} - f_{\mathrm{FEM}} | / f_{\mathrm{FEM}}$. In addition, we compared the circumferential mode shapes of the first four orders calculated with the present method and the FEM when $L_d = 0.75$, as seen in Fig. 2.

From Table 2 and Fig. 2, it is clear that the results obtained with the present method agree quite well with those obtained with FEM. For the first ten-order natural frequencies, the relative errors are less than 1%, which verifies the accuracy of the present method in calculating free vibration.

In order to further demonstrate the accuracy and reliability of the present method, the natural frequencies and mode shapes calculated with the present method are compared with those in Ref. [9] (based on the boundary integral method). The material parameters in Ref. [9] are listed as $E = 206$GPa, $\mu = 0.3$, $\rho = 7680$ kg/m3, and the dimensions of the shell are $L = 0.664$ m, $R = 0.175$ m, and thickness $h = 0.001$ m. The density of the fluid is $\rho_f = 1000$ kg/m^3. The relative error of the natural frequencies calculated with the two methods is defined as Error $= | f_{\mathrm{PM}} - f_{\mathrm{Ref}} | / f_{\mathrm{Ref}}$, where f_{PM} represents the natural frequencies calculated with the present method and f_{Ref} represents the natural frequencies in Ref. [9].

In Table 3, the differences between the results of the present method and Ref. [9] are relatively small (not more than 1%). In Fig. 3, the model shapes further prove that the present method for the free vibration is accurate and reliable. Furthermore, since the fluid and the structure are partially coupled, the sound wave radiated by the structure encounters the sound wave reflected by the free surface, making the sound field very complex. At the same time, the circumferential structural wave is cross-coupling, which makes the mode shapes of the cylindrical shell irregular (as seen in Fig. 3).

Table 3 Comparison of the first six natural frequencies when $L_d = 0.5$

Order number	1	2	3	4	5	6
f_{PM} /Hz	98.9	99.9	128.1	131.8	182.4	184.6
f_{Ref} /Hz	99.9	100.8	129.1	133.1	184.1	185.1
Error	1.00%	0.89%	0.77%	0.98%	0.92%	0.27%

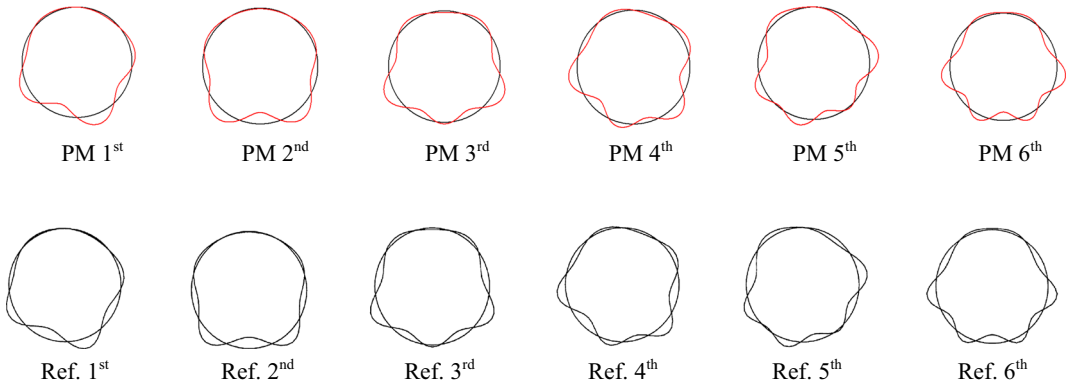

Fig. 3 The circumferential mode shapes of the first six orders when $L_{\mathrm{d}} = 0.5$

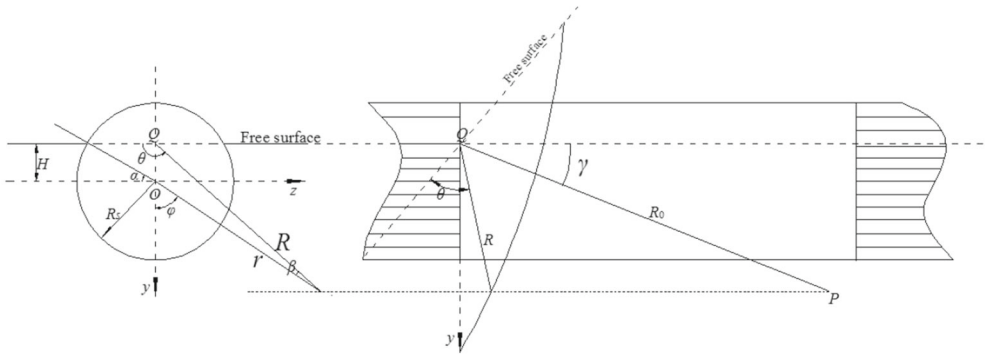

Fig. 4 Model of the rigid barrier-cylindrical shell

4 The far-field sound radiation model

After getting the forced vibration response, the far-field sound pressure can be obtained using the presented method, which combines the Fourier transform technique and the stationary phase method.

Given that the model is the rigid barrier-cylindrical shell model, the model image is shown in Fig. 4. In this model, there are two semi-infinite rigid barrier columns (the velocity is zero). Point P is the far-field observation point, the distance between the point P and Q is R_0, and the included angle between axis x and the vector $\vec{R}_0$ is γ. Simultaneously, the original center of the spherical coordinate system (R_0, γ, θ) is set as the point Q for solving the far-field sound radiation more conveniently.

By transforming the vibration response from the frequency domain to the wavenumber domain, the response function can be rewritten as follows:

$$\tilde{w}(k_x, \varphi) = \sum_{n=-\infty}^{+\infty} \tilde{w}_n(k_x) \exp(in\varphi) \tag{26}$$

where $\tilde{w}_n = (k_x) = \frac{1}{2\pi} \sum_{m=1}^{+\infty} \frac{W_{mn} k_m}{k_m^2 - k_x^2} [1 - (-1)^m \exp(-ik_x L)]$.

And then, assuming that the acoustic boundary satisfies the boundary condition and the Helmholtz equations as follows:

$$\tilde{p}(R,\theta,k_x)=\sum_{j=1}^{+\infty}\tilde{P}_j(k_x)H_j^{(1)}(\tilde{k}_r R)\sin(j\theta) \tag{27}$$

where $\tilde{P}_j(K_x)$ is the amplitude of the sound pressure in the wavenumber domain, $\tilde{k}_r=\sqrt{k_f^2-k_x^2}$ is the radial wavenumber in the wavenumber domain.

By the use of the sound-solid coupled continuous condition which is transformed to the wavenumber domain, the relationship between the sound pressure amplitude and transformation amplitude could be obtained, and the continuous condition can be expressed as:

$$\left.\frac{\partial\tilde{p}}{\partial r}\right|_{r=R_s}=\rho_f\omega^2\tilde{w}(k_x,\varphi) \tag{28}$$

Combining Eqs. (28), (29), and (30), the relationship between the sound pressure amplitude and transformation amplitude can be written by using the Galerkin method as follows:

$$\rho_f\omega^2[\boldsymbol{V}_1]\{\tilde{\boldsymbol{w}}_{\boldsymbol{n}}\}=[\boldsymbol{V}_2]\left\{\tilde{\boldsymbol{P}}_{\boldsymbol{j}}\right\} \tag{29}$$

where $\{\tilde{\boldsymbol{w}}_n\}=[\tilde{w}_{-N}(k_x),\quad \tilde{w}_{-N+1}(k_x)\ldots,\quad \tilde{w}_N(k_x)]^{\mathrm{T}}$, $\left\{\tilde{P}_j\right\}=[\tilde{P}_1(k_x),\quad \tilde{P}_2(k_x)\ldots,\quad \tilde{P}_{2N+1}(k_x)]^{\mathrm{T}}$.

Assuming that the weight function is the radial displacement function, the elements of the matrixes $[\boldsymbol{V}_1]$ and $[\boldsymbol{V}_2]$ can be expressed as:

$$\begin{cases}[\boldsymbol{V}_1]_{a,b}=\int_{-\alpha-\frac{\pi}{2}}^{\alpha+\frac{\pi}{2}}\exp[i(b-1-N)\varphi]\cdot\exp[i(a-1-N)\varphi]\mathrm{d}\varphi\\ [\boldsymbol{V}_2]_{a,b}=\displaystyle\int_{-\alpha-\frac{\pi}{2}}^{\alpha+\frac{\pi}{2}}\tilde{k}_r H_b^{(1)\prime}(\tilde{k}_r R)\sin(b\theta)\cos\beta\cdot\exp[i(a-1-N)\varphi]\mathrm{d}\varphi\\ \qquad\displaystyle+\int_{-\alpha-\frac{\pi}{2}}^{\alpha+\frac{\pi}{2}}bH_b^{(1)}(\tilde{k}_r R)\cos(b\theta)\frac{\sin\beta}{R}\cdot\exp[i(a-1-N)\varphi]\mathrm{d}\varphi\end{cases} \tag{30}$$

where β=3π /2− θ− φ.

The transformed matrix of Eq. (31) can be written as:

$$\left\{\tilde{\boldsymbol{P}}_{\boldsymbol{j}}\right\}=[Tran]\{\tilde{\boldsymbol{w}}_{\boldsymbol{n}}\} \tag{31}$$

where the order of the matrix $[Tran]$ is $2N+1$, and $[Tran]=\rho_f\omega^2[\boldsymbol{V}_2]^{-1}[\boldsymbol{V}_1]$。

And applying the inverse Fourier transformation, the expression of the sound pressure can be obtained as the infinite integrates:

$$p(R,\theta,x)=\int_{-\infty}^{+\infty}\sum_{j=1}^{+\infty}\tilde{P}_j(k_x)H_j^{(1)}(\tilde{k}_r R)\sin(j\theta)\exp(ik_x x)\mathrm{d}k_x \tag{32}$$

Due to the approximate expansion of the Hankel function in the analysis of the far-field sound radiation, the sound pressure can be written as the approximate form:

$$p(R,\theta,x)=\int_{-\infty}^{+\infty}\sum_{j=1}^{+\infty}\tilde{P}_j(k_x)\sqrt{\frac{2}{\pi\tilde{k}_r R}}\exp[i(\tilde{k}_r R-\frac{j\pi}{2}-\frac{\pi}{4})]\sin(j\theta)\exp(ik_x x)\mathrm{d}k_x \tag{33}$$

Transforming Eq. (35) to the spherical coordinate system, the sound pressure could be described as:

$$p(R_0,\theta,\gamma)=\int_{-\infty}^{+\infty}\sum_{j=1}^{+\infty}\tilde{P}_j(k_x)\sqrt{\frac{2}{\pi\tilde{k}_r R_0\sin\gamma}}\sin(j\theta)\exp[-i(\frac{\pi}{4}+\frac{j\pi}{2})]\times\exp[i(k_x R_0\cos\gamma+\tilde{k}_r R_0\sin\gamma)]\mathrm{d}k_x \tag{34}$$

By the use of the stationary phase method, the infinite integral can be solved, and the stationary phase point $k_s = k_f \cos\gamma$ can be obtained. The final expression of the sound pressure is:

$$p(R_0, \theta, \gamma) = \frac{-2i \exp(ik_f R_0)}{R_0} \sum_{j=1}^{+\infty} \tilde{P}_j(k_f \cos\gamma) \sin(j\theta) \exp(-i\frac{j\pi}{2}) \tag{35}$$

Combining Eqs. (28), (33), (35) and substituting the stationary phase point into Eqs. (28), (33), the far-field sound pressure can be solved.

5 Results and discussion

The following parameters of the coupling model are used in the calculation: $E = 206$GPa, $\mu = 0.3$, $\rho = 7850$ kg/m^3, $\rho_f = 1025$ kg/m^3, $c_f = 1500$ m/s, $L = 1.284$ m, $R_s = 0.18$ m, $h = 0.003$ m. The complex elastic modulus of the shell is expressed as $E' = E(1 + i\eta)$, where the structural damping factor $\eta = 0.01$.

The location of the point exciting force is assumed as $x_0 = L/2$, $\varphi_0 = \pi$ And the force amplitude is assumed as $F_0 = 1$. The far-field sound pressure can be obtained with the exciting frequencies of 300 Hz and 600 Hz and the immersion depth of $-$ 0.09 m and 0.09 m. After calculation by the present method, the results are compared with the results which got by the BEM as shown in Fig. 5. The far-field observation point is set as $R_0 = 1000$ m, observation angle $\gamma = \pi/3$, $\theta = 0 \sim \pi (\varphi = -\pi/2 \sim \pi/2)$.

As seen from Fig. 5, the results obtained by the present method have good agreement with those obtained by the BEM. So it is believed that the present method is accurate. Besides, since there is only a simple algebraic summation in Eq. (35), the efficiency of the stationary phase method is higher than the BEM.

As shown in Fig. 6, the far-field sound pressures are presented as functions of the exciting frequency. The location and amplitude of the exciting force are assumed as $x_0 = L/2$, $\varphi_0 = \pi$, and $F_0 = 1$. In addition, the observation point is set as $\gamma = \pi/3$, $\theta = \pi/4$ and $\pi/2$. It can be seen from Fig. 6 that the far-field sound pressure values of $\theta = \pi/4$ and $\pi/2$ at different frequencies are relatively close, which is consistent with the law shown in Fig. 5.

For different exciting frequencies, the far-field sound pressures can be calculated by the present method. Figure 7 shows the difference in the circumferential distribution of far-field sound pressure at the different exciting frequencies. The sound pressures are calculated for $\gamma = \pi/3$ and the $L_d = 0.75$,0.25. It is clear from these figures that the directivity of far-field sound pressure varies with the immersed depth and the frequency. Moreover, the petal number of the directivity increases with the frequency increase.

As shown in Fig. 8, it is the directivity of far-field sound pressure when the cylindrical shell is located at different immersed depths at the frequencies $f = 200$,600,800 and 3000 Hz, respectively. As seen in the sound pressure directivity curves in Fig. 8, the maximum sound pressure is always at a = 0, directly under the shell. Moreover, the directivity curves are symmetrical about the vertical axis of symmetry ($\theta = \pi/2$). These could be explained by the image method [6]. Because the observation point is far from the cylindrical shell, the submerged radiation surface could be assumed as a point radiation source. Due to the free surface, the far-field sound pressure is superimposed by the part directly produced by the real source and the other part reflected by the free surface according to the image method. The reflected part could be assumed that produced by the mirror image source. In this case, the distance between the real source and the image source is so close that the physical model could be seen as a dipole model. So that the dipole could be expressed as:

$$P = \frac{A}{R} \exp\left(-ik_f R\right)\left[-2i \sin\left(k_f D \sin\theta\right)\right] \tag{36}$$

where A is the sound pressure amplitude, R is the distance between the field and origin points, and D represents the distance between the real source and the image source. The value of $k_f D$ is minor than $\pi/2$, when the exciting frequency is low. Therefore, the sound pressure is maxed at the $\theta = \pi/2$. The symmetry can also be obtained in Eq. (36) according to the characteristic of the sine function.

6 Conclusion

This paper proposes a new method to solve the vibration and far-field sound radiation of partially submerged cylindrical shells. Conclusions are summarized in the following:

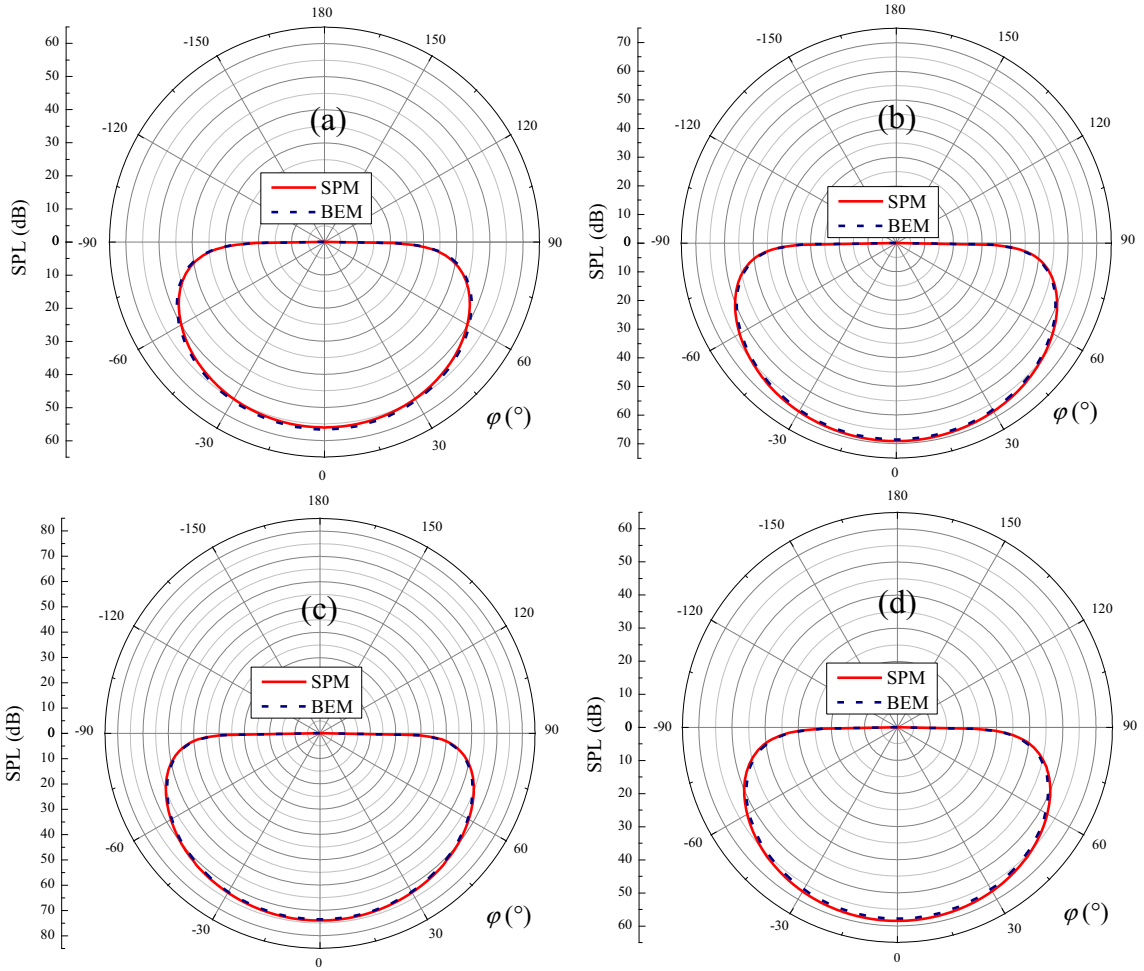

Fig. 5 Comparison of the results obtained by the stationary phase method (SPM) and BEM with different frequencies and immersion depth **a** $f = 300$ Hz, $H = -0.09$ m; **b** $f = 600$ Hz, $H = -0.09$ m; **c** $f = 300$ Hz, $H = 0.09$ m; **d** $f = 600$ Hz, $H = 0.09$ m;

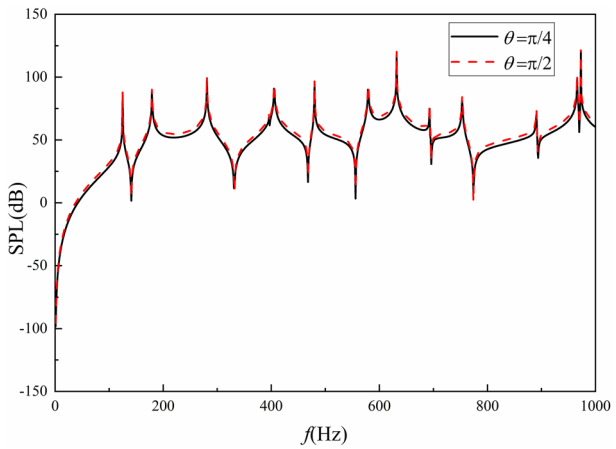

Fig. 6 The far-field sound pressure in the region $\gamma = \pi/3$ and$\theta = \pi/4$,$\pi/2$ due to a point force on the shell

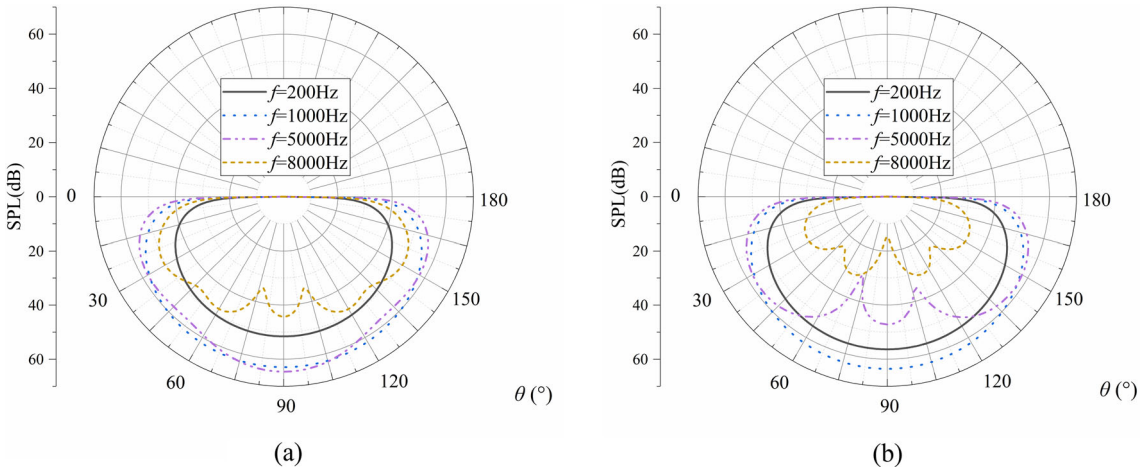

Fig. 7 The circumferential distribution of far-field sound pressure at different exciting frequencies: **a** $L_d = 0.75$; **b** $L_d = 0.25$

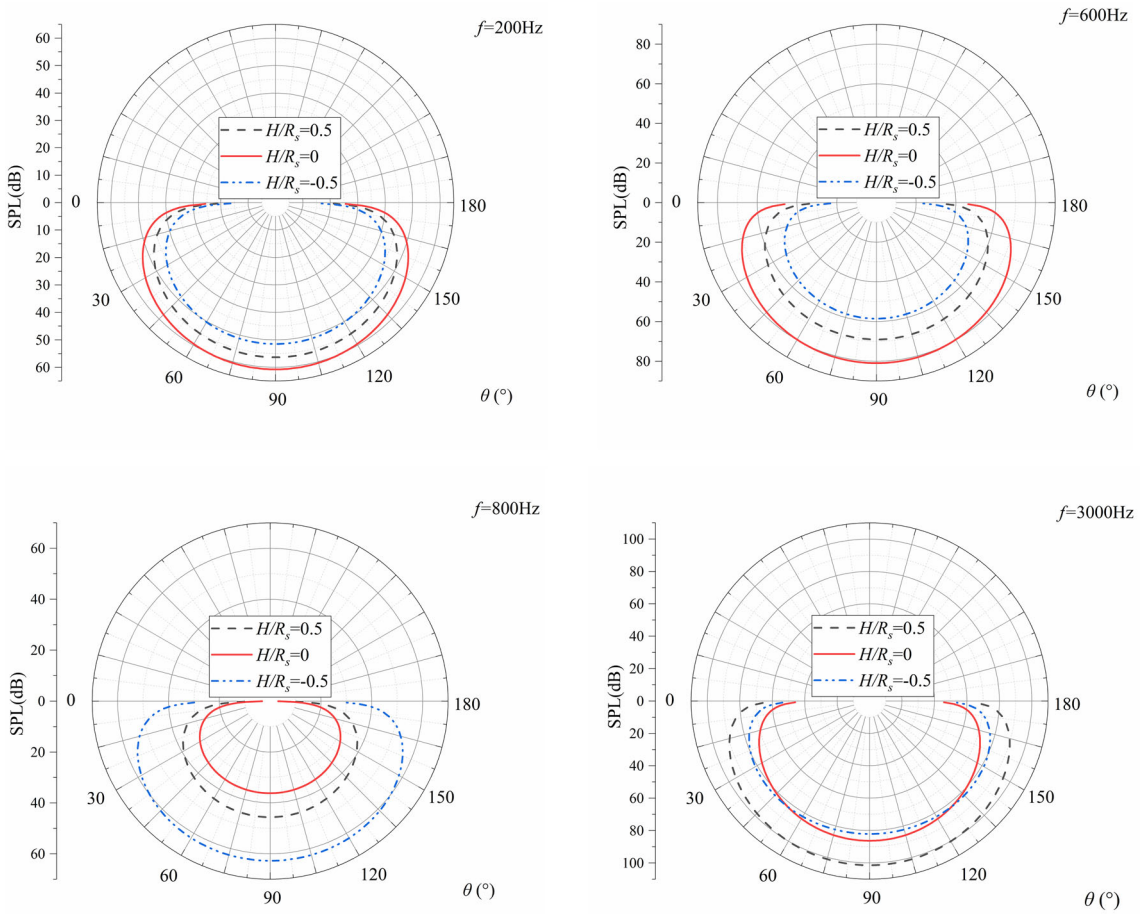

Fig. 8 The circumferential distribution of far-field sound pressure at different immersed depths

(1) The accuracy of the proposed method is verified by comparing the cylindrical shell's vibration and acoustic radiation between the proposed method and the finite element method. Moreover, the present method demonstrated a broader application scope of the immersed depth than the previous analytical method.
(2) The increase in the free surface height leads to an increase in the fluid–structure interface. In turn, this increased the added mass of the fluid–structure system, which reduced the natural frequencies of the coupled cylindrical shell.
(3) A model for the far-field sound radiation was introduced, combining the method with the stationary phase approach. And the present method was shown to have superior accuracy and efficiency concerning the boundary element method.
(4) The directivity of far-field sound pressure varies with the immersed depth and the frequency. And the petal number of the directivity increases with the frequency increase. Besides, the sound pressure is maxed at the $\theta = \pi/2$ when the exciting frequency is low. The directivity curves are also symmetrical about the vertical axis of symmetry ($\theta = \pi/2$).

Acknowledgements The authors wish to express their gratitude to the National Natural Science Foundation of China (Contract Nos. 51839005, 51879113), the Youth Science Foundation of Jiangxi province (Contract No. 20202BABL214049), and the Youth Science Foundation of Jiangxi Provincial Education Department (Contract No. GJJ190339). All data included in this study are available upon request by contact with the corresponding author.

References

1. Fuller, C.R., Fahy, F.J.: Characteristics of wave propagation and energy distributions in cylindrical elastic shells filled with fluid. J. Sound Vib. **81**, 501–518 (1982). https://doi.org/10.1016/0022-460X(82)90293-0
2. Zhang, X.M., Liu, G.R., Lam, K.Y.: Coupled vibration analysis of fluid-filled cylindrical shells using the wave propagation approach. Appl. Acoust. **62**, 229–243 (2001). https://doi.org/10.1016/S0003-682X(00)00045-1
3. Zhong Wang, X., Ban Jiang, C., YangXu, R.: Structural and acoustic response of a finite stiffened submarine hull. China Ocean Eng. **30**, 898–915 (2016). https://doi.org/10.1007/s13344-016-0058-y
4. Zhang, X.M.: Frequency analysis of submerged cylindrical shells with the wave propagation approach. Int. J. Mech. Sci. **44**, 1259–1273 (2002). https://doi.org/10.1016/S0020-7403(02)00059-0
5. Guo, W., Li, T., Zhu, X., Miao, Y., Zhang, G.: Vibration and acoustic radiation of a finite cylindrical shell submerged at finite depth from the free surface. J. Sound Vib. **393**, 338–352 (2017). https://doi.org/10.1016/j.jsv.2017.01.003
6. Guo, W., Li, T., Zhu, X.: Far-field acoustic radiation and vibration of a submerged finite cylindrical shell below the free surface based on energy functional variation principle and stationary phase method. Noise Control Eng. J. **65**, 565–576 (2017)
7. Chen, L., Liang, X., Yi, H.: Vibro-acoustic characteristics of cylindrical shells with complex acoustic boundary conditions. Ocean Eng. **126**, 12–21 (2016). https://doi.org/10.1016/j.oceaneng.2016.08.028
8. Guo, W., Li, T., Zhu, X., Miao, Y.: Sound-structure interaction analysis of an infinite-long cylindrical shell submerged in a quarter water domain and subject to a line-distributed harmonic excitation. J. Sound Vib. **422**, 48–61 (2018). https://doi.org/10.1016/j.jsv.2018.02.031
9. Ergin, A., Temarel, P.: Free vibration of a partially liquid-filled and submerged, horizontal cylindrical shell. J. Sound Vib. **254**, 951–965 (2002). https://doi.org/10.1006/jsvi.2001.4139
10. Brunner, D., Junge, M., Cabos, C., Gaul, L.: Vibroacoustic simulation of partly immersed bodies by a coupled fast BE-FE approach. J. Acoust. Soc. Am. **123**, 3418 (2008)
11. Khojasteh Kashani, B., Aftabi Sani, A.: Free vibration analysis of horizontal cylindrical shells including sloshing effect utilizing polar finite elements. Eur. J. Mech. A/Solids. **58**, 187–201 (2016). https://doi.org/10.1016/j.euromechsol.2016.02.002
12. Seybert, A., Wu, T.: Modified Helmholtz integral equation for bodies sitting on an infinite plane. J. Acoust. Soc. Am. **85**, 19–23 (1989). https://doi.org/10.1121/1.397716
13. Yildizdag, M.E., Ardic, I.T., Kefal, A., Ergin, A.: An isogeometric FE-BE method and experimental investigation for the hydroelastic analysis of a horizontal circular cylindrical shell partially filled with fluid. Thin-Walled Struct. **151**, 106755 (2020). https://doi.org/10.1016/j.tws.2020.106755
14. Junge, M., Brunner, D., Becker, J., Gaul, L.: Interface-reduction for the Craig-Bampton and Rubin method applied to FE–BE coupling with a large fluid–structure interface. Int. J. Numer. Methods Eng. **77**, 1731–1752 (2009)
15. Seilsepour, H., Zarastvand, M., Talebitooti, R.: Acoustic insulation characteristics of sandwich composite shell systems with double curvature: the effect of nature of viscoelastic core. J. Vib. Control. (2022). https://doi.org/10.1177/10775463211056758
16. Zarastvand, M.R., Asadijafari, M.H., Talebitooti, R.: Acoustic wave transmission characteristics of stiffened composite shell systems with double curvature. Compos. Struct. **292**, 115688 (2022). https://doi.org/10.1016/j.compstruct.2022.115688
17. Gohari, H.D., Zarastvand, M.R., Talebitooti, R., Loghmani, A., Omidpanah, M.: Radiated sound control from a smart cylinder subjected to piezoelectric uncertainties based on sliding mode technique using self-adjusting boundary layer. Aerosp. Sci. Technol. **106**, 106141 (2020). https://doi.org/10.1016/j.ast.2020.106141

18. Rahmatnezhad, K., Zarastvand, M.R., Talebitooti, R.: Mechanism study and power transmission feature of acoustically stimulated and thermally loaded composite shell structures with double curvature. Compos. Struct. **276**, 114557 (2021). https://doi.org/10.1016/j.compstruct.2021.114557
19. Zarastvand, M.R., Ghassabi, M., Talebitooti, R.: Acoustic insulation characteristics of shell structures: a review. Arch. Comput. Methods Eng. **28**, 505–523 (2021). https://doi.org/10.1007/s11831-019-09387-z
20. Zhao, K., Fan, J., Wang, B., Tang, W.: Analytical and experimental study of the vibro-acoustic behavior of a semi-submerged finite cylindrical shell. J. Sound Vib. **482**, 115466 (2020). https://doi.org/10.1016/j.jsv.2020.115466
21. Li, T.Y., Wang, P., Zhu, X., Yang, J., Ye, W.B.: Prediction of far-field sound pressure of a semisubmerged cylindrical shell with low-frequency excitation. J. Vib. Acoust. Trans. ASME. **139**, 041002 (2017). https://doi.org/10.1115/1.4036209
22. Ergin, A.: An approximate method for the free vibration analysis of partially filled and submerged, horizontal cylindrical shells. J. Sound Vib. **207**, 761–767 (1997). https://doi.org/10.1006/jsvi.1997.1133
23. Selmane, A., Lakis, A.A.: Vibration analysis of anisotropic open cylindrical shells subjected to a flowing fluid. J. Fluids Struct. **11**, 111–134 (1997). https://doi.org/10.1006/jfls.1996.0069
24. Amabili, M.: Free vibration of partially filled, horizontal cylindrical shells. J. Sound Vib. **191**, 757–780 (1996). https://doi.org/10.1006/jsvi.1996.0154
25. Amabili, M.: Flexural vibration of cylindrical shells partially coupled with external and internal fluids. J. Vib. Acoust. Trans. ASME. **119**, 476–484 (1997). https://doi.org/10.1115/1.2889748
26. Santisteban Hidalgo, J.A., Gama, A.L., Moreira, R.M.: Natural vibration frequencies of horizontal tubes partially filled with liquid. J. Sound Vib. **408**, 31–42 (2017). https://doi.org/10.1016/j.jsv.2017.07.011
27. Escaler, X., De La Torre, O., Goggins, J.: Experimental and numerical analysis of directional added mass effects in partially liquid-filled horizontal pipes. J. Fluids Struct. **69**, 252–264 (2017). https://doi.org/10.1016/j.jfluidstructs.2017.01.001
28. Sun, H., Zhang, A., Li, H.: Experimental study and dynamic characteristics analysis of partially liquid-filled annulus tubes. PLoS ONE **13**, e0209011 (2018). https://doi.org/10.1371/journal.pone.0209011
29. Guo, W., Li, T., Zhu, X., Qu, K.: Semi-analytical research on acoustic-structure coupling calculation of partially submerged cylindrical shell. Acta Phys. Sin. **67**, 084302 (2018)
30. Guo, W., Feng, Q., Li, T., Zhu, X., Miao, Y.: A new solution for vibroacoustic analysis of two-dimensional cylindrical shells partially liquid-filled or partially submerged in fluid. Mech. Syst. Signal Process. **140**, 106685 (2020). https://doi.org/10.1016/j.ymssp.2020.106685
31. W., Soedel. Vibrations of shells and plates, Vibrations of shells and plates, 1981.